Phase and Structural Behaviour of the PrAlO₃–SmAlO₃ System

T. Basyuk^a, L. Vasylechko^a, S. Fadeev^a, V. Berezovets^b, D. Trots^c and R. Niewa^d

^{a}Lviv Polytechnic National University, 12 Bandera St., 79013 Lviv, Ukraine

^{b}Karpenko Physico-Mechanical Institute, 5 Naukova St., 79601 Lviv, Ukraine

^{c}Bayerisches Geoinstitut, Universität Bayreuth, Universitätsstr. 30, 95447 Bayreuth, Germany

^{d}Institut für Anorganische Chemie, Universität Stuttgart, Pfaffenwaldring 55, 70569 Stuttgart, Germany

High resolution *in situ* X-ray powder diffraction applying synchrotron radiation and differential thermal analysis/scanning calorimetry methods have been used to examine the pseudo-binary system $PrAlO_3$–$SmAlO_3$. Two kinds of solid solutions with rhombohedral and orthorhombic structure exist at room temperature. At elevated temperatures, a continuous phase transition $Pm\bar{3}m \leftrightarrow R\bar{3}c$ and a first-order transformation $R\bar{3}c \leftrightarrow Pbmn$ occur in the two respective phases. A sequence of low-temperature phase transformations $R\bar{3}c \leftrightarrow Imma \leftrightarrow C2/m$ has been detected in $Pr_{1-x}Sm_xAlO_3$ samples with $x < 0.35$. Based on *in situ* powder diffraction and differential thermal analysis/scanning calorimetry data, the phase diagram of the pseudo-binary system $PrAlO_3$–$SmAlO_3$ has been constructed.

PACS numbers: 61.05.Cp, 61.50.Ks, 81.30.Bx

1. Introduction

At room temperature, praseodymium and samarium aluminates, $PrAlO_3$ and $SmAlO_3$, adopt two different distortion variants of the cubic perovskite structure: one with rhombohedral symmetry $R\bar{3}c$ and one with orthorhombic, space group $Pbnm$. At elevated temperatures both compounds undergo structural phase transitions. $PrAlO_3$ with rhombohedral structure continuously transforms to the cubic perovskite structure at 1770 K [1–5], whereas a first-order phase transition from an orthorhombic to a rhombohedral structure occurs in $SmAlO_3$ within the temperature range of 1023–1058 K [6–8]. One more phase transition from the rhombohedral to the cubic perovskite structure was observed in $SmAlO_3$ at 2223 K [7]; however, this transition has not been confirmed by other research groups.

Low-temperature (LT) structure examinations performed by means of *in situ* synchrotron powder diffraction revealed that $SmAlO_3$ remains orthorhombic down to 12 K [5, 9]. In contrast, praseodymium aluminate undergoes additional phase transformations below room temperature (RT): a first-order transition from the rhombohedral to an orthorhombic structure at 205 K and a second-order transformation from the orthorhombic to a monoclinic structure at 151 K [10–14]. These transitions are considered to be caused by electronic effects involving Pr^{3+} ions, such as the coupling between Pr^{3+} electronic states and phonons, as well as cooperative Jahn–Teller effects. In addition to these transformations, several authors reported an additional transition to a tetra-gonal structure around 118 K, which was considered to be due to the coupling between acoustic phonons and temperature-dependent optical modes [11, 15–19]. However, based on a combination of high-resolution neutron and synchrotron powder diffraction data, it could be shown that the symmetry remains monoclinic down to 10 K, although $PrAlO_3$ becomes metrically tetragonal within experimental resolution below 118 K [20]. According to [21], the acoustic and optical anomalies around 118 K appear to be associated with this metrically tetragonal structure that develops as accidental strain degeneracy between 110 and 120 K. A somewhat different interpretation of the LT structural behaviour of $PrAlO_3$ was given by other authors [22, 23]. According to these studies, the $PrAlO_3$ structure successively transforms from a rhombohedral structure in $R\bar{3}c$ (phase II) to an orthorhombic in $Imma$ (phase III), followed by a further orthorhombic phase in $Imma$ (phase IV) and a tetragonal one in $I4/mcm$ (phase V) at 215, 153, and 122 K, respectively. The phases III and IV are described as having a similar orthorhombic structure both in space group $Imma$, but with a different scheme of AlO_6 octahedra tilting angles.

The unusual structural behaviour of $PrAlO_3$ below RT has provoked a number of publications in the last decades, and the discussions concerning LT transitions and the structures of the LT modifications of $PrAlO_3$ are not settled even today [5].

The aim of the present study is to enlighten the phase and structural behaviour in the $PrAlO_3$–$SmAlO_3$ pseudo-

-binary system in a wide temperature range of 12–1173 K by using high resolution *in situ* X-ray powder diffraction applying synchrotron radiation and differential thermal analysis/scanning calorimetry (DTA/DSC) methods.

2. Experimental and data analysis

Series of the $Pr_{1-x}Sm_xAlO_3$ samples with x in the range of 0.12–0.92 were prepared from the oxides Pr_6O_{11}, Sm_2O_3 and Al_2O_3 according to the following reaction scheme:

$$(1-x)Pr_6O_{11} + 3xSm_2O_3 + 3Al_2O_3$$

$$= 6Pr_{1-x}Sm_xAlO_3 + (1-x)O_2.$$
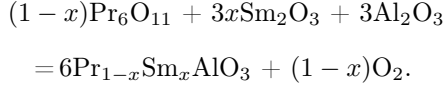
Appropriate amounts of the previously fired oxides were mixed and pressed to pellets. The pellets were subsequently loaded into alumina crucibles and annealed in air at 1300 K for 24 h. In a final synthesis step the sintered pellets were arc-melted in Ar atmosphere.

Phase and structural characterisation of the samples at room temperature was performed by X-ray powder diffraction using a Huber image plate Guinier camera G670 (Cu K_{α_1} radiation, $\lambda = 1.54056$ Å). High--temperature DTA and DSC measurements were performed on an STA 409 thermal analyser (NETZSCH, Selb) with a SiC-furnace under static air atmosphere. DTA curves were measured with a Pt10%Rh–Pt sensor in Al_2O_3 crucibles in the temperature range of 300 K to 1773 K and with heating rates of 10 and 20 K/min. A high-temperature DSC sensor was used for higher sensitivity measurements in Al_2O_3 sample pans up to 1573 K. Typically, the phase transitions were indicated by broad signals with no significant hysteresis. Transition temperatures were extracted from the onset of the thermal signal in the heating cycles. For LT examination, difference scanning calorimetry was performed on a DSC 204 Phoenix (Netzsch, Selb) in sealed aluminum crucibles. Temperature calibration was carried out with five transition temperatures of pure materials. The temperature was varied in the range of 90 K to 310 K with heating/cooling rates of 5, 10 and 20 K/min.

In situ low- and high-temperature crystal structure investigations were carried out with high-resolution powder diffraction applying synchrotron radiation (beamline B2, HASYLAB at DESY). Both LT and HT diffraction experiments were performed in the Debye–Scherrer capillary geometry using an on-site readable image plate detector OBI [24]. The wavelengths of 0.49342 Å (LT experiments) and 0.48917 Å (HT measurements) were calibrated using the reflection positions of silicon (NIST SRM 640b) and/or LaB_6 (NIST SRM 660a) reference materials. The typical full width at half maximum (FWHM) of reflections obtained in this geometry was 0.06–0.08°. A closed-cycle cryostat [25] and a STOE furnace were used for *in situ* LT and HT diffraction experiments, respectively. All crystallographic calculations (refinements of the lattice parameters as well as full profile structure refinements) were performed by means of the

Windows version of the Crystal Structure Determination program package WinCSD [26].

3. Results

From the results of the XRD phase and crystal structural analysis it was established that two kinds of solid solutions $Pr_{1-x}Sm_xAlO_3$ with rhombohedral ($x \leq 0.30$) and orthorhombic ($x \geq 0.40$) structures exist at RT. A narrow immiscibility gap exists between these two perovskite-type phases. The morphotropic phase transition in the $PrAlO_3$–$SmAlO_3$ system occurs at $x = 0.35$, where the coexistence of both phases was detected. A similar transition in the related $NdAlO_3$–$SmAlO_3$ system takes place around the samarium content of $x = 0.27$ [8, 27]. Structural parameters of both modifications of $Pr_{1-x}Sm_xAlO_3$ solid solutions at RT, obtained by full-profile Rietveld refinements, are collected in Table I. The concentration dependence of the cell dimensions is presented in Fig. 1. All lattice parameters decrease monotonically with increasing Sm content in $Pr_{1-x}Sm_xAlO_3$ and a strong anisotropy in the lattice contraction is observed for the orthorhombic phase. In agreement with Vegard's law an almost linear dependence is observed for the normalized cell volume.
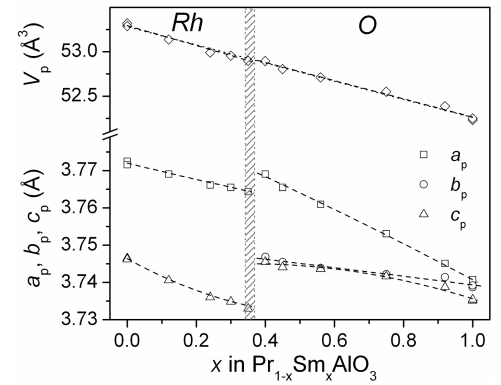

Fig. 1. Concentration dependences of normalized lattice parameters and cell volumes of $Pr_{1-x}Sm_xAlO_3$ solid solutions at room temperature. Lattice parameters and cell volumes of the rhombohedral (Rh) and orthorhombic $Pbnm$ ($O1$) cells are normalized to the perovskite ones as follows: $a_p = a_r/\sqrt{2}$, $c_p = c_r/\sqrt{12}$, $V_p = V_r/6$; $a_p = a_o/\sqrt{2}$, $b_p = b_o/\sqrt{2}$; $c_p = c_o/2$, $V_p = V_o/4$.

At elevated temperatures, a first-order transformation from the orthorhombic to a rhombohedral structure is observed in the $Pr_{1-x}Sm_xAlO_3$ samples with $x = 0.92$, 0.75, and 0.56 at 930 K, 723 K and 500 K, respectively. This transition was found in both DTA/DCS measurements and *in situ* X-ray synchrotron powder diffraction patterns. As an example, Fig. 2 shows the temperature dependences of the normalized lattice parameters and the cell volume of the $Pr_{0.25}Sm_{0.75}AlO_3$ sample. The limitation of the equipment used did not allow to detect the HT rhombohedral-to-cubic phase transition, which hypothetically occurs above 1700 K. From the temperature

dependences of lattice parameters of the rhombohedral phase such transitions are predicted to take place in the temperature range of 1900–2400 K.

From the extrapolation of the c/a parameter ratios of the rhombohedral phases, the temperatures of the continuous transition $R\bar{3}c \leftrightarrow Pm\bar{3}m$ were estimated for all $Pr_{1-x}Sm_xAlO_3$ samples (see, for example, Fig. 3). It was found that the transition temperatures increase linearly with increasing Sm content. A similar behavior of the transition temperature is also typical for the above mentioned first-order structural transformation $R\bar{3}c \leftrightarrow Pbnm$.

TABLE I

Structural parameters of different modifications of $Pr_{1-x}Sm_xAlO_3$ solid solution at RT.

Atom, sites	Parameters	$x = 0.12$ $R\bar{3}c$	$x = 0.24$ $R\bar{3}c$	$x = 0.30$ $R\bar{3}c$	$x = 0.56$ $Pbnm$	$x = 0.75$ $Pbnm$	$x = 0.92$ $Pbnm$
	a [Å]	5.32876(5)	5.32619(3)	5.32311(4)	5.3181(1)	5.3058(1)	5.2948(2)
	b [Å]	–	–	–	5.2941(1)	5.2913(1)	5.2906(2)
	c [Å]	12.9550(2)	12.9429(1)	12.9334(1)	7.4851(2)	7.4804(2)	7.4756(2)
Pr(Sm), 6a in $R\bar{3}c$ 4c in $Pbnm$	x	0	0	0	−0.0035(6)	−0.0039(6)	−0.0045(5)
	y	0	0	0	0.0155(3)	0.0204(2)	0.0237(2)
	z	1/4	1/4	1/4	1/4	1/4	1/4
	B_{iso} [Å²]	0.58(2)	0.91(2)	0.93(2)	0.63(3)	0.70(3)	0.63(3)
Al, 6b in $R\bar{3}c$ 4b in $Pbnm$	x	0	0	0	1/2	1/2	1/2
	y	0	0	0	0	0	0
	z	0	0	0	0	0	0
	B_{iso} [Å²]	1.19(9)	0.82(7)	0.62(6)	1.89(12)	1.54(11)	1.24(10)
O1, 18e in $R\bar{3}c$ 4c in $Pbnm$	x	0.5531(15)	0.5494(7)	0.5526(8)	0.073(3)	0.093(4)	0.090(3)
	y	0	0	0	0.481(4)	0.477(4)	0.474(3)
	z	1/4	1/4	1/4	1/4	1/4	1/4
	B_{iso} [Å²]	2.6(2)	0.86(8)	0.79(9)	2.4(5)	3.3(6)	2.1(5)
O2, 8d in $Pbnm$	x	–	–	–	−0.274(5)	−0.276(4)	−0.274(4)
	y	–	–	–	0.278(5)	0.263(5)	0.267(5)
	z	–	–	–	0.031(2)	0.032(2)	0.029(2)
	B_{iso} [Å²]	–	–	–	2.4(3)	1.6(3)	1.4(3)

Both DTA/DSC data and *in situ* synchrotron powder diffraction examinations reveal a sequence of LT phase transformations in the praseodymium-rich samples $Pr_{1-x}Sm_xAlO_3$ with $x < 0.35$, whereas the samples with higher samarium content remain orthorhombic and isotypic with GdFeO$_3$ down to 12 K. Analysis of the corresponding diffraction data allows to establish the following sequence of the transitions: $R\bar{3}c \leftrightarrow Imma \leftrightarrow C2/m$, which is similar to that occurring in PrAlO$_3$. The observed sequence of LT structural transformations is clearly illustrated by the temperature dependences of the lattice parameters for the example of $Pr_{0.70}Sm_{0.30}AlO_3$ (Fig. 4). Refined crystallographic parameters of all structural modifications of $Pr_{1-x}Sm_xAlO_3$ solid solutions at different temperatures are presented in Table II.

Isomorphic substitution of Sm for Pr differently affects the LT transition temperatures in $Pr_{1-x}Sm_xAlO_3$. The temperature of the orthorhombic-to-monoclinic phase transition decreases linearly with decreasing Pr content, whereas for the rhombohedral-to-orthorhombic transformation some increase of the transition temperature is observed. In this respect, the system studied differs from the related PrAlO$_3$–RAlO$_3$ and CeAlO$_3$–RAlO$_3$ (R = La, Nd) systems, in which the temperatures of all LT transitions drop with decreasing praseodymium (cerium) content [28–32].

Based on the results of *in situ* synchrotron powder diffraction examinations and partially of DTA/DSC measurements as well as available literature data, the phase diagram of the pseudo-binary system PrAlO$_3$–SmAlO$_3$ has been constructed (Fig. 5). Five kinds of solid solutions with different perovskite-type crystal structures exist in the system, depending on composition and temperature. Similar to the first members of the RAlO$_3$ series (R = La, Ce, Pr, Nd) and pseudo-binary solid solutions among them [5, 30–32], the mixed praseodymium–
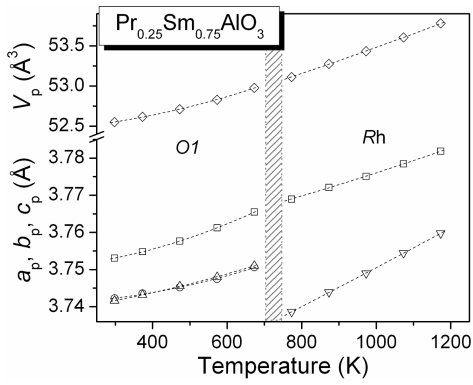
Fig. 2. Temperature dependences of normalized lattice parameters and cell volumes of orthorhombic $Pbnm$ ($O1$) and rhombohedral (Rh) phases of $Pr_{0.25}Sm_{0.75}AlO_3$.
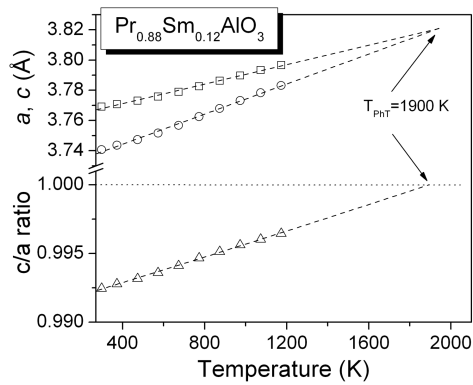

Fig. 3. Lattice parameters and their ratio of rhombohedral $Pr_{0.88}Sm_{0.12}AlO_3$ in the temperature range of 300–1200 K and extrapolation to the expected phase transition to the cubic structure.
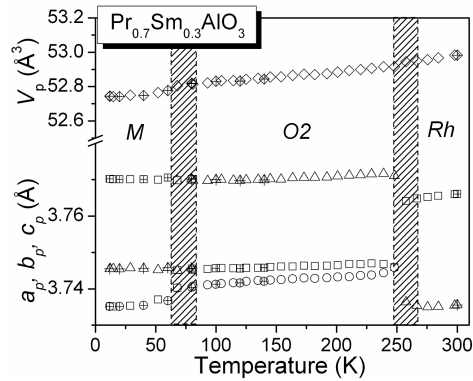

Fig. 4. Low-temperature dependences of the normalized lattice parameters and cell volumes of monoclinic (M), orthorhombic $Imma$ ($O2$), and rhombohedral (Rh) phases of $Pr_{0.7}Sm_{0.3}AlO_3$, obtained on cooling and heating (open and crossed symbols, respectively).
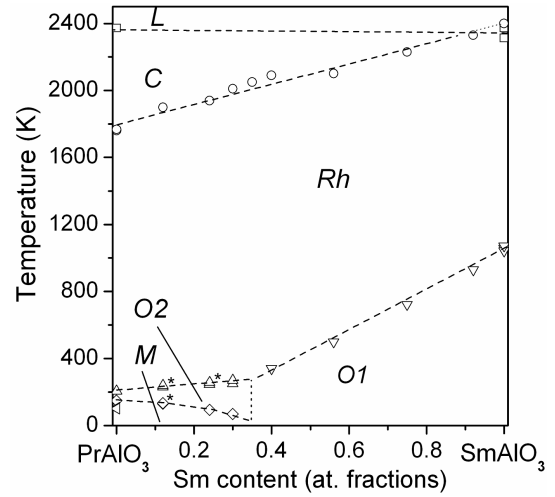

Fig. 5. Phase diagram of the pseudo-binary system $PrAlO_3$–$SmAlO_3$. The letters L, C, Rh, $O1$, $O2$ and M designate liquid, cubic, rhombohedral, orthorhombic $Imma$, orthorhombic $Pbnm$ and monoclinic phase fields, respectively. The symbols * denote the data obtained from DTA/DSC experiments. Transition temperatures for $PrAlO_3$ and $SmAlO_3$ are taken from the literature [2, 4, 7, 8, 18, 20–22].

samarium aluminates $Pr_{1-x}Sm_xAlO_3$ with $x < 0.9$ crystallize in the cubic perovskite structure at high temperatures, which on cooling transforms into a rhombohedral structure. The solid solution with the cubic structure exists in a relatively narrow temperature range between the liquidus (solidus) lines and $Pm\bar{3}m \leftrightarrow R\bar{3}c$ transition temperature, which increase linearly with Sm content. Thus, the temperature range of existence of the cubic $Pr_{1-x}Sm_xAlO_3$ phase converges with increasing Sm content and vanishes when $x \to 0.9$. The compositions with $x > 0.9$ seem to crystallize in the rhombohedral perovskite structure from the melt at high temperatures as is known for $SmAlO_3$. For the latter composition, the rhombohedral-to-cubic phase transition is predicted to occur at about 2450 K, which is above the melting point of the compound. The rhombohedral perovskite phase in the $PrAlO_3$–$SmAlO_3$ system exists in a broad temperature range of 210–2320 K depending on the composition. A continuous solid solution covering the whole concentration range occurs between 1060 K and 1760 K. The orthorhombic structure in $Pbnm$ is inherent only for $Pr_{1-x}Sm_xAlO_3$ compositions with $x > 0.35$. With rising Sm content the maximum temperature of existence of solid solutions with this crystal structure increases from 340 K to 1060 K. Finally, solid solutions with orthorhombic ($Imma$) and monoclinic structures have very limited concentration and temperature existence ranges: they occur only for compositions with $x < 0.35$ and below 270 K.

TABLE II

Crystallographic data for different modifications of $Pr_{1-x}Sm_xAlO_3$.
S.G. = space group.

Lattice parameters [Å]	Atoms, sites	x	y	z	B_{iso} [Å^2]
$Pr_{0.88}Sm_{0.12}AlO_3$, $T = 573$ K, S.G. $R\overline{3}c$, $R_I = 0.0662$, $R_P = 0.1317$					
$a = 5.33979(7)$ $c = 12.9961(2)$	Pr(Sm), $6a$	0	0	1/4	1.02(1)
	Al, $6b$	0	0	0	0.89(5)
	O, $18e$	0.5396(11)	0	1/4	0.75(10)
$Pr_{0.25}Sm_{0.75}AlO_3$, $T = 573$ K, S.G. $Pbnm$, $R_I = 0.0849$, $R_P = 0.1435$					
$a = 5.31926(7)$ $b = 5.29983(8)$ $c = 7.4961(1)$	Pr(Sm), $4c$	−0.0048(3)	0.0163(1)	1/4	1.084(7)
	Al, $4b$	1/2	0	0	0.995(3)
	O1, $4c$	0.075(2)	0.488(2)	1/4	1.0(2)
	O2, $8d$	−0.269(2)	0.271(3)	0.0267(14)	1.0(11)
$Pr_{0.70}Sm_{0.30}AlO_3$, $T = 205$ K, S.G. $Imma$, $R_I = 0.0713$, $R_P = 0.1193$					
$a = 5.2983(1)$ $b = 7.4866(1)$ $c = 5.33298(9)$	Pr(Sm), $4e$	0	1/4	0.5030(3)	0.736(5)
	Al, $4b$	0	0	0	0.63(2)
	O1, $4e$	0	1/4	0.063(2)	0.86(15)
	O2, $8g$	1/4	−0.0312(7)	1/4	0.49(9)
$Pr_{0.70}Sm_{0.30}AlO_3$, $T = 60$ K, S.G. $I2/m$, $R_I = 0.0671$, $R_P = 0.1380$					
$a = 5.3316(1)$ $b = 7.4740(2)$ $c = 5.2968(1)$ $\beta = 90.290(2)$	Pr(Sm), $4i$	0.2503(7)	0	0.7513(7)	0.751(4)
	Al, $4e$	1/4	1/4	1/4	0.84(3)
	O1, $4i$	0.183(2)	0	0.220(3)	0.6(1)
	O2, $4g$	0	0.274(2)	0	0.6(2)
	O3, $4h$	1/2	0.217(2)	0	0.628(3)

4. Conclusion

The crystal structures of solid solutions $Pr_{1-x}Sm_xAlO_3$ and their thermal behaviour in a wide temperature range have been investigated by using *in situ* X-ray powder diffraction applying synchrotron radiation and DTA/DSC techniques. It was established that five kinds of solid solutions with different types of perovskite structures exist in the $PrAlO_3$–$SmAlO_3$ system, depending on composition and temperature. At elevated temperatures, two phase transitions occur in $Pr_{1-x}Sm_xAlO_3$: a continuous transformation $R\overline{3}c \leftrightarrow Pm\overline{3}m$ and a first-order transition $Pbnm \leftrightarrow R\overline{3}c$. The temperatures of both transitions increase linearly with substitution of Sm for Pr, in accordance with decreasing average R-cation radii and Goldschmidt tolerance factor. Two LT structural transformations $R\overline{3}c \leftrightarrow Imma$ and $Imma \leftrightarrow C2/m$, which are observed in the $PrAlO_3$–$SmAlO_3$ system below 270 K, occur only in the Pr-rich samples. It is evident that, similarly to $PrAlO_3$, these transitions are caused by electronic effects involving Pr^{3+} ions and the transition temperatures depend on the Pr content in corresponding solid solutions. However, in contrast to the related $PrAlO_3$–$LaAlO_3$ and $PrAlO_3$–$NdAlO_3$ systems, in which the transition temperatures fall with decreasing praseodymium content, a substitution of Sm for Pr in $Pr_{1-x}Sm_xAlO_3$ leads to gradual increase of $R\overline{3}c \leftrightarrow Imma$ transition temperatures and decrease of the $Imma \leftrightarrow C2/m$ temperatures. Similar behaviour is also observed in the related $PrAlO_3$–$EuAlO_3$ and $PrAlO_3$–$YAlO_3$ systems [33]. It is evident that such complex behaviour of the LT phase transitions in the $PrAlO_3$–$RAlO_3$ systems upon rare-earth metal substitution requires more comprehensive investigations of the $PrAlO_3$-based materials by using various experimental techniques as well as theoretical calculations.

References

[1] S. Geller, V.B. Bala, *Acta Crystallogr.* **9**, 1019 (1956).

[2] J.F. Scott, *Phys. Rev.* **183**, 823 (1969).

[3] S. Geller, P.M. Raccah, *Phys. Rev. B* **2**, 1167 (1970).

[4] C.J. Howard, B.J. Kennedy, B.C. Chakoumakos, *J. Phys., Condens. Matter* **12**, 349 (2000).

[5] L. Vasylechko, A. Senyshyn, U. Bismayer, in: *Handbook on the Physics and Chemistry of Rare Earths,* Vol. 39, Eds. K.A. Gschneidner, Jr., J.-C.G. Bünzli, V.K. Pecharsky, North-Holland, Netherlands 2009, p. 113.

[6] P.A. Arsenev, L.M. Kovba, Kh.S. Bagdasarov, B.F. Dzhurinskii, A.V. Potemkin, B.I. Pokrovskii, F.M. Spiridonov, A.V. Antonov, V.V. Ilyukhin, *Compounds of Rare Earth Elements. Systems with the Oxides of I–III Group Elements*, Nauka, Moscow 1983 (in Russian).

[7] J. Coutures, J.P. Coutures, *J. Solid State Chem.* **52**, 95 (1984).

[8] A. Yoshikawa, A. Saitow, H. Horiuchi, T. Shishido, T. Fukuda, *J. Alloys Comp.* **266**, 104 (1998).

[9] L. Vasylechko, A. Senyshyn, D. Savytskii, M. Knapp, C. Bähtz, U. Bismayer, *HASYLAB Ann. Rep.* **1**, 407 (2004).

[10] E. Cohen, L.A. Riseberg, W.A. Norland, R.D. Burbank, R.C. Sherwood, L.G. van Uitert, *Phys. Rev.* **186**, 476 (1969).

[11] R.T. Harley, W. Hayes, A.M. Perry, S.R.P. Smith, *J. Phys. C, Solid State Phys* **6**, 2382 (1973).

[12] R.J. Birgeneau, J.K. Kjems, G. Shirane, L.G. Van Uitert, *Phys. Rev. B* **10**, 2512 (1974).

[13] K.B. Lyons, R.J. Birgeneau, E.I. Blount, L.G. Van Uitert, *Phys. Rev. B* **11**, 891 (1975).

[14] A.P. Young, *J. Phys. C, Solid State Phys.* **8**, 3158 (1975).

[15] P.A. Fleury, P.D. Lazay, L.G. Van Uitert, *Phys. Rev. Lett.* **33**, 492 (1974).

[16] M.D. Sturge, E. Cohen, L.G. Van Uitert, R.P. Van Stapele, *Phys. Rev. B* **11**, 4768 (1975).

[17] D.J. Benard, W.C. Walker, *Phys. Status Solidi* **18**, 717 (1976).

[18] R.T. Harley, *J. Phys. C, Solid State Phys.* **10**, 205 (1977).

[19] M. D'Iorio, W. Berlinger, J.G. Bednorz, K.A. Mueller, *J. Phys. C, Solid State Phys.* **17**, 2293 (1984).

[20] S.M. Moussa, B.J. Kennedy, B.A. Hunter, C.J. Howard, T. Vogt, *J. Phys., Condens. Matter* **13**, 203 (2001).

[21] M.A. Carpenter, C.J. Howard, B.J. Kennedy, K.S. Knight, *Phys. Rev. B* **72**, 024118 (2005).

[22] H. Fujii, M. Hidaka, B.M. Wanklyn, *Phase Transit.* **70**, 115 (1999).

[23] S. Watanabe, M. Hidaka, H. Yoshizawa, B.M. Wanklyn, *Phys. Status Solidi B* **243**, 424 (2006).

[24] M. Knapp, V. Joco, C. Baehtz, H.H. Brecht, A. Berghaeuser, H. Ehrenberg, H. von Seggern, H. Fuess, *Nucl. Instrum. Methods Phys. Res. A* **521**, 565 (2004).

[25] J. Ihringer, A. Koster, *J. Appl. Crystallogr.* **26**, 135 (1993).

[26] G.L. Akselrud, P.Yu. Zavalij, Yu. Grin, V.K. Pecharsky, B. Baumgartner, E. Woelfel, *Mater. Sci. Forum* **133**, 335 (1993).

[27] A. Saitow, A. Yoshikawa, H. Horiuchi, T. Shishido, T. Fukuda, M. Tanaka, T. Mori, S. Sasaki, *J. Appl. Crystallogr.* **31**, 663 (1998).

[28] T.J. Glynn, R.T. Harley, W. Hayes, A.J. Rushworth, R.H. Smith, *J. Phys. C, Solid State Phys.* **8**, 126 (1975).

[29] W.A. Nordland, L.G. Van Uitert, *J. Phys. Chem. Solids* **31**, 1257 (1970).

[30] T. Basyuk, L. Vasylechko, I.I. Syvorotka, U. Schmidt, D. Trots, R. Niewa, *Phys. Status Solidi C* **6**, 1008 (2009).

[31] T. Basyuk, L. Vasylechko, S. Fadeev, I.I. Syvorotka, D. Trots, R. Niewa, *Radiat. Phys. Chem.* **78(10)**, Suppl. 1, S97 (2009).

[32] L. Vasylechko, A. Senyshyn, D. Trots, R. Niewa, W. Schnelle, M. Knapp, *J. Solid State Chem.* **180**, 1277 (2007).

[33] T.V. Basyuk, L.O. Vasylechko, I.I. Syvorotka, V. Berezovets, S.V. Fadeev, *Bull. Lviv Polytech. Natl. Univ., Electronics* **646**, 3 (2009) (in Ukrainian).